Available online at www.sciencedirect.com

SciVerse ScienceDirect

Ceramics International 38 (2012) 2295–2304

CERAMICS INTERNATIONAL

www.elsevier.com/locate/ceramint

Synthesis, characterization and alcohol sensing property of Zn-doped SnO_2 nanoparticles

R.K. Mishra, P.P. Sahay *

Department of Physics, Motilal Nehru National Institute of Technology, Allahabad 211 004, India

Received 14 October 2011; received in revised form 27 October 2011; accepted 28 October 2011
Available online 4 November 2011

Abstract

The Zn-doped SnO_2 nanoparticles synthesized by the chemical co-precipitation route and having dopant concentration varying from 0 to 4 at%, were characterized by X-ray diffraction (XRD) and transmission electron microscopy (TEM) for structural and morphological studies. XRD analyses reveal that all the samples are polycrystalline SnO_2 having tetragonal rutile structure with nanocrystallites in the range 10–25 nm. The TEM images show agglomeration of grains (cluster of primary crystallites). A corresponding selected area electron diffraction pattern reveals the different Debye rings of SnO_2, as analyzed in XRD. Alcohol sensing properties of all the Zn-doped samples were investigated for various concentrations of methanol, ethanol and propan-2-ol in air at different operating temperatures. Among all the samples examined, the 4 at% Zn-doped sample exhibits the best response to different alcohol vapors at the operating temperature of 250 °C. For a concentration of 50 ppm, the 4 at% Zn-doped sample shows the maximum response 85.6% to methanol, 87.5% to ethanol and 94.5% to propan-2-ol respectively at the operating temperature of 250 °C. A possible reaction mechanism of alcohol sensing has been proposed.

Keywords: SnO_2 nanoparticles; Structural properties; Alcohol sensing; Sensor response

1. Introduction

Tin oxide (SnO_2), an important n-type wide direct band gap semiconductor (E_g = 3.67 eV at 300 K), has been the subject of great interest for researchers because of its numerous and wide-ranging applications, such as in flat panel displays, catalysis, heat mirrors, transparent electrodes preparation, gas sensing, etc. [1–7]. More recently, this material has received a growing attention as a nanostructured material due to its interesting electrical and optical properties arising out of large surface-to-volume ratio, quantum confinement effect, etc. [8–12]. Morphology, size and size distribution of SnO_2 nanoparticles play an important role in deciding their properties. One important method to modify the characteristics of the nanoparticles is the introduction of dopants in the parent system, which, in turn, influences the performance of the gas sensors based on these nanoparticles. Various dopants like Al, In, Cu, etc. have been used to improve sensitivity and selectivity performance of the gas sensors based on the SnO_2 nanoparticles [13–15]. Ménini et al. [13] have investigated the CO response of a nanostructured SnO_2 gas sensor doped with palladium and platinum. Microstructure In/Pd-doped SnO_2 sensor for low-level CO detection has been studied by Zhang et al. [14]. Thomas et al. [15] have examined the influence of Cs doping in spray deposited SnO_2 thin films for LPG sensors.

Though a large number of studies on the gas sensors based on SnO_2 nanoparticles (in various forms) have been carried out, but to the best of our knowledge, a very little attention has been paid to the investigation of the Zn-doped SnO_2 nanoparticles for gas sensing applications [16]. In recent times, environmental regulations for VOCs have been tightened all over the world. At high concentrations in air, VOCs with their speedy evaporation and toxic or carcinogenic nature are extremely dangerous to human beings [17]. Alcohols (methanol, ethanol and propan-2-ol) are widely used in many applications. Among them, methanol is highly toxic and often fatal to human beings, whereas excessive exposure of propan-2-ol results in headache, dizziness, nausea, vomiting, etc. Thus, seeing the importance of health risks, the alcohol sensing properties of the Zn-doped SnO_2 nanoparticles have been investigated and reported in this

* Corresponding author. Tel.: +91 532 2271260; fax: +91 532 2545341.
E-mail address: dr_ppsahay@rediffmail.com (P.P. Sahay).

0272-8842/$36.00
doi:10.1016/j.ceramint.2011.10.081

paper. For a material to be used as a chemical gas sensor, it should exhibit high response at low operating temperatures and the low concentrations of tested gases. Keeping this in view, the low concentrations (10–50 ppm) of alcohols were tested.

To prepare active nanocrystalline powders, several chemical techniques have been investigated and reported in the literature. Among the various methods of preparing nanostructured SnO_2, co-precipitation [18], sol–gel [19], spray pyrolysis [20], hydrothermal routes [21], etc. are popular. In the present investigation, we have used co-precipitation method for the preparation of Zn-doped SnO_2 nanoparticles as this method requires little manipulation and no sophisticated equipment.

2. Experimental

The Zn-doped SnO_2 nanoparticles were synthesized by the chemical co-precipitation route. All the chemicals used were of analytical grade. Firstly, stannic tetrachloride hydrated ($SnCl_4{\cdot}5H_2O$) was dissolved in distilled water to prepare 0.1 M solution. Zinc acetate dihydrate [$Zn(CH_3COO)_2{\cdot}2H_2O$] was then added to the solution as the source of Zn-dopant. The dopant concentration (at% Zn to Sn) was varied from 0 to 4 at%. Ammonia solution was then added into the solution under constant agitation to form white slurry. The slurry was filtered and washed thoroughly with distilled water several times to remove the chloride ions completely from the precipitate. The resulting precipitate was dried at 90 °C and then calcined at 600 °C for 10 h in air. The dried mass was then crushed into fine powder. The structural analysis of the SnO_2 powder was carried out using PANalytical X'Pert Pro X-ray Diffractometer with Cu Kα radiation (λ = 1.5418 Å) as X-ray source at 40 kV and 30 mA in the scanning angle (2θ) from 20° to 65°. The morphologies and dimensions of the powders were determined by transmission electron microscopy (TEM) which was done on a Philips model Tecnai-20 using an accelerating voltage of 200 kV.

The fine powders, both undoped and Zn-doped, separately were pressed into pellets of 12 mm diameter and 2.5 mm thickness at a pressure of ∼15 MPa using a hydraulic press. These pellets were sintered at around 600 °C for 5 h in air. High temperature silver paste was used for making ohmic contacts on the two flat surfaces of the sintered pellets. The alcohol sensing properties of the pellets were carried out in an experimental set up shown in Fig. 1. The experimental set-up was so designed that there was a complete dry air (free from humidity) in the surrounding areas of the experimental films to be examined. Therefore, the effect of humidity on the sensor response has not been taken into account in the present investigation. The pellet was mounted on a home-made two-probe assembly which was inserted coaxially inside a resistance-heated furnace. The temperature of the pellet was monitored using a chromel–alumel thermocouple with the help of a Motwane digital multimeter (Model: 454). The electrical resistance of the pellet was measured before and after exposure to alcohol vapour by a 6½ Digit USB Digital Multimeter (Keithley Model: 2100). The measurement of alcohol concentration was carried out by taking required amount of liquid alcohol in a Hamilton micro syringe and then injecting it into the enclosure. The response of the pellet towards alcohol vapour was studied at different operating temperatures in the range 150–250 °C for various concentrations ranging from 10 ppm to 50 ppm in air.

3. Results and discussion

3.1. Structural and morphological studies

XRD patterns of the 0 at%, 1 at%, 2 at%, 3 at% and 4 at% Zn-doped SnO_2 nanoparticles are shown in Fig. 2. All the diffraction peaks in the pattern can be indexed as the tetragonal rutile structure of the polycrystalline SnO_2 in the standard data (JCPDS File No. 72-1147) for samples. No phase corresponding to zinc or other zinc compound is found in the pattern. It is

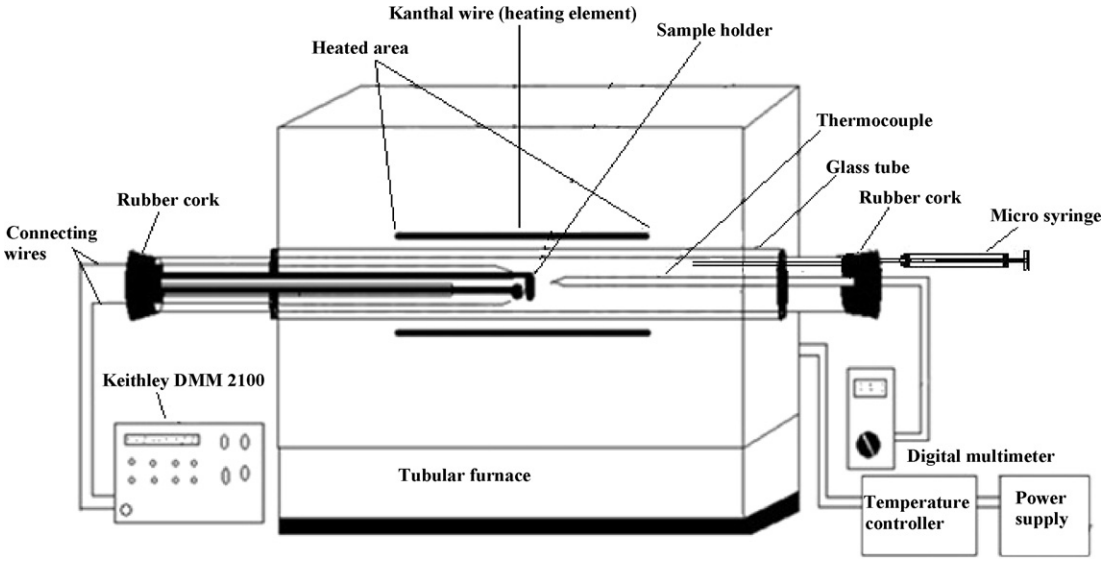

Fig. 1. Experimental set-up for alcohol sensing studies.

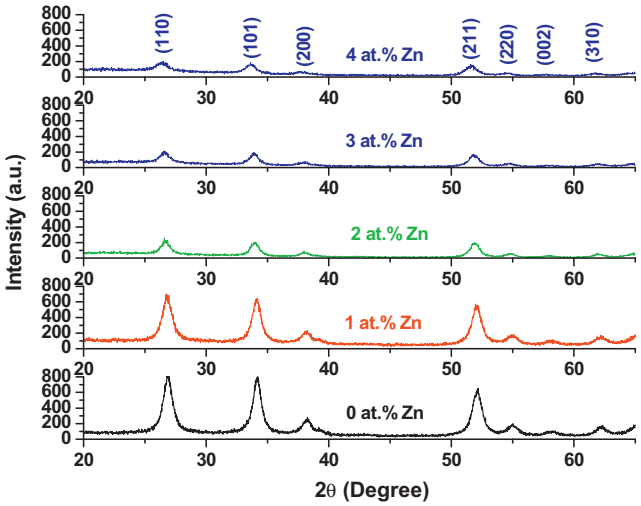

Fig. 2. XRD spectra of the 0 at%, 1 at%, 2 at%, 3 at% and 4 at% Zn-doped SnO_2 nanoparticles.

observed that the intensities of all the peaks are diminished on doping with zinc, indicating their lower crystallinity as compared with the undoped SnO_2 nanoparticles. Poor crystallinity in the Zn-doped nanoparticles is attributed to the fact that the Zn incorporation in the parent system enables more nucleation sites which, in turn, inhibit the growth of crystal grains, resulting increase in the lattice strain.

Another effect of Zn doping in SnO_2 nanoparticles is the shift of the diffraction peak positions towards lower values of 2θ compared to the peak position observed in the undoped sample. Such a decrease in 2θ arises due the fact that the ionic radii of Zn^{2+} and Sn^{4+} are 0.074 and 0.069 nm, respectively and therefore the lattice spacing (d) between the planes is expected to increase when the Zn^{2+} ions are substituted into the Sn^{4+} sites in the parent system. This is found in agreement with the XRD results where d-spacing of the lattice planes in the zinc doped samples increases.

The lattice constants ($a = b$, and c) have been calculated from the most prominent peaks using the equation [22]:

$$\frac{1}{d^2} = \frac{(h^2 + k^2)}{a^2} + \frac{l^2}{c^2} \tag{1}$$

The crystallite size (D) and the lattice strain (ε) of the SnO_2 nanoparticles have been determined using the Debye–Scherrer formula (2) [22] and the tangent formula (3) [22]:

$$D = \frac{0.9\lambda}{(\beta\cos\theta)} \tag{2}$$

$$\varepsilon = \frac{\beta}{4\tan\theta} \tag{3}$$

where λ is the X-ray wavelength equal to 1.5406 Å, θ is the Bragg diffraction angle and β (radians) is the full-width at half maximum.

The lattice constants, the crystallite size and the lattice strain thus obtained are listed in Table 1. It is observed that the crystallite size of the SnO_2 nanoparticles decreases on Zn doping. This is due to enhancement in the densities of nucleation centres in the doped samples which results in the formation of smaller crystallites [23]. The lattice constants, a and c, are found to increase with the zinc doping. This is attributed to the replacement of Sn^{4+} ions by Zn^{2+} ions during formation of the Zn doped SnO_2 nanoparticles since the radius of Zn^{2+} ion is larger than that of Sn^{4+} ion ($r_{Zn}{}^{2+} = 0.074$ nm and $r_{Sn}{}^{4+} = 0.069$ nm).

The porosity (P) (listed in Table 1) of the sintered pellets has been determined using the equation [24]:

$$P = \left(1 - \frac{\rho_a}{\rho_x}\right) \times 100\% \tag{4}$$

where

$$\rho_x = \frac{nM}{Na^2c} \tag{5}$$

and

$$\rho_a = \frac{m}{v} = \frac{m}{\pi r^2 h} \tag{6}$$

Here, n is the number of molecules per unit cell, M the molecular weight, a and c the lattice parameters, N the Avogadro's number while m, v, r, and h are the mass, volume, radius, and thickness of the pellet respectively.

The bright-field TEM images and the corresponding selected area electron diffraction (SAED) patterns of the synthesized SnO_2 nanoparticles are shown in Fig. 3(a–c). It is clear from the figures that the grains are segregated together to form large sized agglomerates (cluster of primary crystallites). The TEM images reveal that the Zn doped samples present smaller particle sizes than the undoped sample (listed in Table 1). A corresponding selected area electron diffraction pattern (shown in the inset) reveals the different Debye rings of SnO_2, as analyzed in XRD.

3.2. Alcohol sensing studies

On exposing the sample to alcohol vapour of desired concentration in air to be examined, the pellet resistance was

Table 1
Structural properties of the undoped and Zn-doped SnO_2 nanoparticles.

S. no.	SnO_2 nanoparticles	a (Å)	c (Å)	Crystallite size (D, nm)	Lattice strain (ε)	Porosity (%)	Particle size by TEM (nm)
1.	Undoped (0 at% Zn)	4.685	3.163	25	0.0065	52.9	37.4
2.	1 at% Zn	4.707	3.166	13	0.0085	61.7	19.3
3.	2 at% Zn	4.721	3.178	17	0.0071	57.4	22.7
4.	3 at% Zn	4.721	3.187	15	0.0083	54.5	–
5.	4 at% Zn	4.784	3.194	11	0.0108	51.8	–

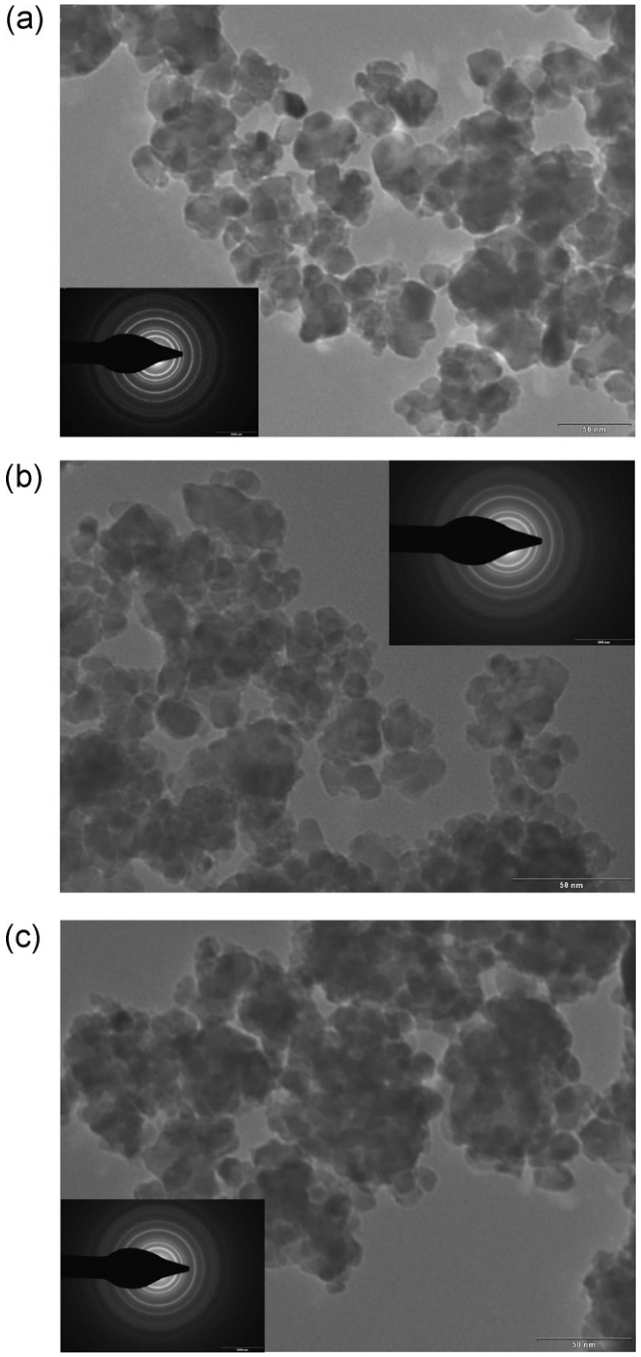

Fig. 3. (a–c) Bright-field TEM images and the selected area electron diffraction (SAED) patterns of the 0 at%, 1 at% and 2 at% Zn-doped SnO_2 nanoparticles.

found to decrease. When the pellet was exposed to air, the pellet resistance recovered its original value. In the present investigation, the sensor response (S) has been defined as the ratio of change in pellet resistance upon exposure to alcohol to the pellet resistance in air (at the same operating temperatures) and is given by the equation:

$$S = \frac{R_a - R_g}{R_a} \times 100\% \quad (7)$$

where R_a is the pellet resistance in air and R_g is the resistance upon exposure to alcohol vapour.

It is well accepted that the response of the semiconductor gas sensors is attributed to the chemisorption of oxygen on the oxide surface and the subsequent reaction between adsorbed oxygen species and tested gas, which causes the resistance change [25]. The same mechanism has been used to explain the alcohol-sensing properties of the SnO_2 nanoparticles.

3.2.1. Methanol sensing

Fig. 4(a–e) presents the methanol response characteristics of the Zn-doped SnO_2 nanoparticles as a function of the operating temperatures. In case of the undoped sample, at lower concentrations the response first increases rapidly with the operating temperature up to 175 °C and thereafter increases slowly. At lower concentrations, there is a sparse surface coverage of methanol molecules on the sample which react effectively with the available oxygen species resulting a rapid increase in response. On the other hand, at higher concentrations there is a dense surface coverage of methanol molecules which prevents subsequent adsorption of atmospheric oxygen and therefore there is a gradual change in response. The 1 at% Zn doped sample begins to attain saturation at the higher operating temperatures beyond 200 °C for all concentrations, whereas the other Zn-doped samples show a tendency of enhanced response with the operating temperature beyond 200 °C for all concentrations. The increase in response is found to be most pronounced in case of the 4 at% Zn doped sample. Variation in response with the operating temperature as well as the methanol concentration depends on the availability of atmospheric oxygen species on the sample surface and the chemical activation of methanol molecules at different operating temperatures. Adsorption of atmospheric oxygen on the sample surface mainly depends on the operating temperature and the surface-to-volume ratio of the crystallites. Among all the samples examined, the 4 at% Zn doped sample show the maximum response (85.6%) at 250 °C for a concentration of 50 ppm methanol in air.

When the sample is heated in ambient at a temperature higher than 150 °C, at first atmospheric oxygen is absorbed on the surface of SnO_2. The adsorption of oxygen forms ionic species such as O^{2-}, O_2^- and O^- which acquire electrons from the semiconducting layer and which desorb from the surface at 80, 150 and 500 °C, respectively. The reaction kinetics is as follows [5,26]:

$$O_2(\text{air}) \leftrightarrow O_2(\text{ads}) \quad (8)$$

$$O_2(\text{ads}) + e^- \leftrightarrow O_2^-(\text{ads}) \quad (9)$$

$$O_2^-(\text{ads}) + e^- \leftrightarrow 2O^-(\text{ads}) \quad (10)$$

The possible reaction mechanism of methanol molecules with the adsorbed oxygen species may be written as follows [27]:

$$CH_3OH(\text{gas}) + O^-(\text{ads}) \rightarrow CH_2O + H_2O + e^- \quad (11)$$

$$CH_2O + O(\text{bulk}) \rightarrow HCOOH + O(\text{vacancies}) \quad (12)$$

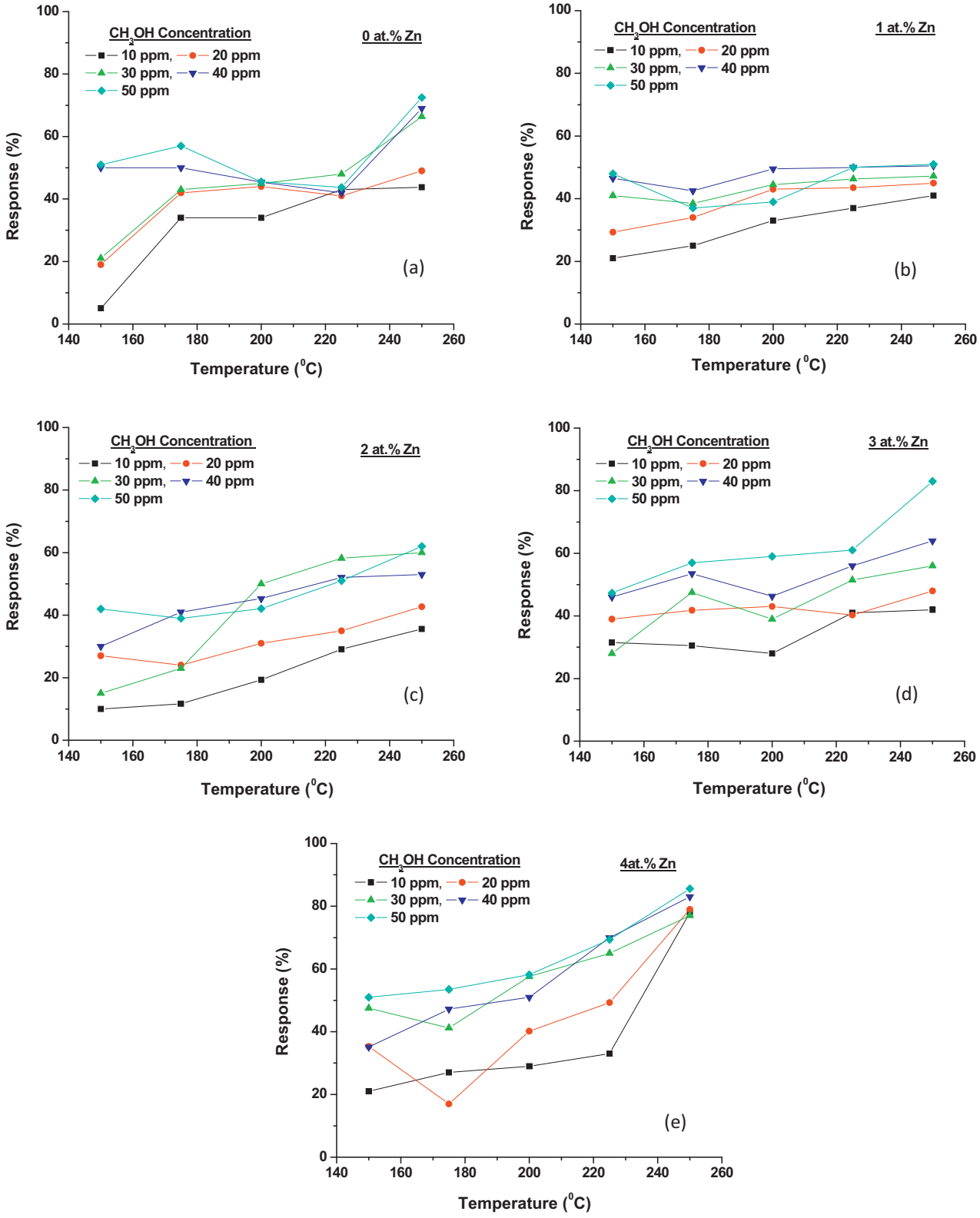

Fig. 4. (a–e) Methanol response characteristics of the 0 at%, 1 at%, 2 at%, 3 at% and 4 at% Zn-doped SnO_2 nanoparticles as a function of operating temperature.

Here, methanol is oxidized to formaldehyde and subsequently formic acid, and liberates electrons into the conduction band, thereby decreasing the resistance of the pellet upon exposure to methanol vapour.

3.2.2. *Ethanol sensing*

Fig. 5(a–e) presents the ethanol response characteristics of the Zn-doped SnO_2 nanoparticles as a function of the operating temperatures at various concentration of ethanol in air. Here, in

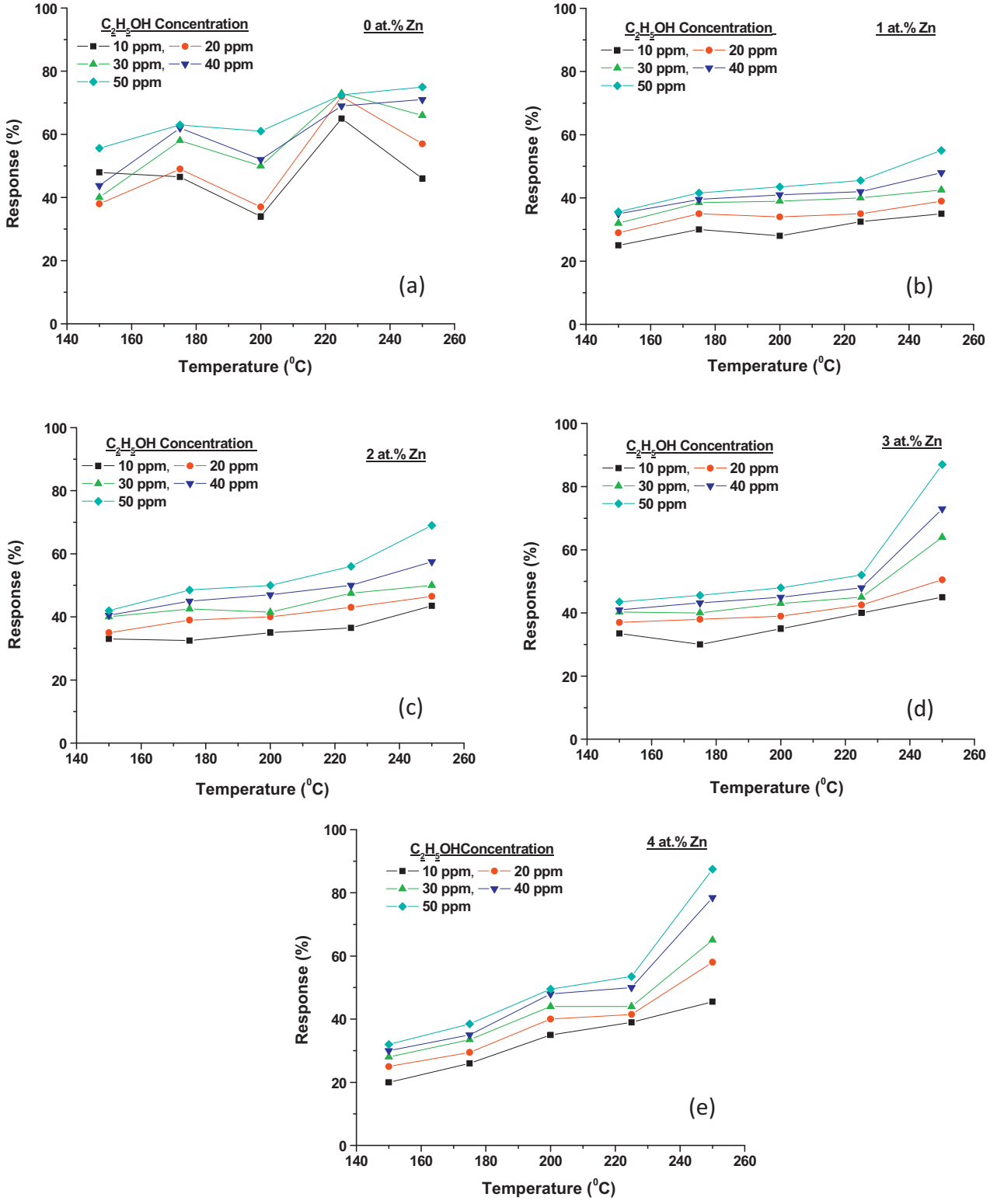

Fig. 5. (a–e) Ethanol response characteristics of the 0 at%, 1 at%, 2 at%, 3 at% and 4 at% Zn-doped SnO_2 nanoparticles as a function of operating temperature.

all the Zn-doped samples, the response increases steadily with the operating temperature at all the concentrations. However, for 3 and 4 at% Zn doped samples, the increase in response is fast in the higher temperature region 225–250 °C. This is because of greater adsorption of atmospheric oxygen at the higher operating temperatures in case of the 3 and 4 at% Zn-doped samples due to their smaller crystallite sizes. In this case, the maximum response 87.5% is observed at the operating temperature of 250 °C for an ethanol concentration of 50 ppm.

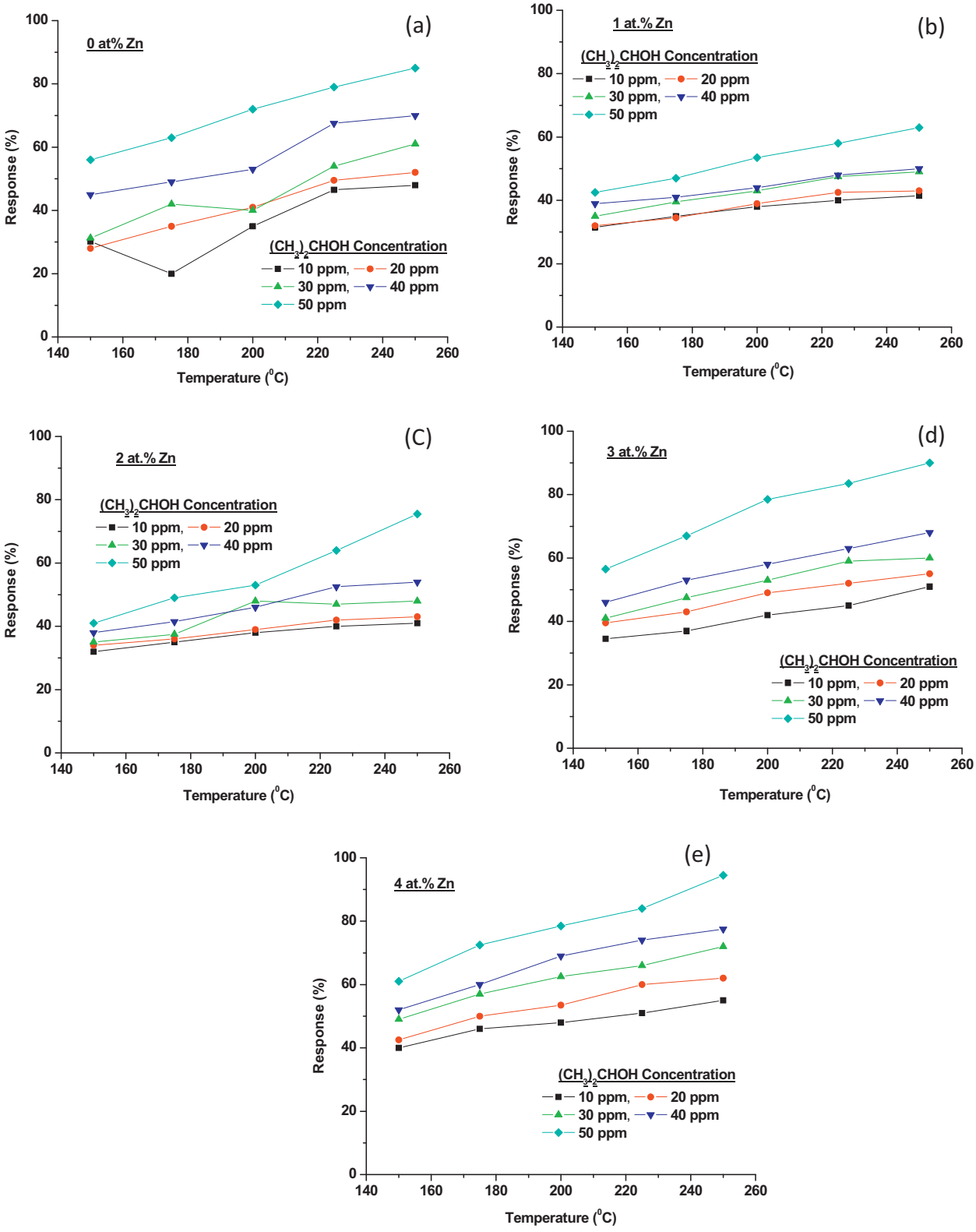

Fig. 6. (a–e) Propan-2-ol response characteristics of the 0 at%, 1 at%, 2 at%, 3 at% and 4 at% Zn-doped SnO_2 nanoparticles as a function of operating temperature.

The possible reaction mechanism of ethanol molecules with the adsorbed oxygen species may be written as follows [28,29]:

$$CH_3CH_2OH(gas) + O^- \rightarrow CH_3CHO + H_2O + e^- \quad (13)$$

$$CH_3CHO + O(bulk) \rightarrow CH_3COOH + O(vacancies) \quad (14)$$

In this case, the formation of acetaldehyde and subsequently acetic acid due to the oxidation of ethanol, leads to the liberation of electrons into the conduction band, resulting in a decrease in the sample resistance.

3.2.3. Propan-2-ol sensing

Fig. 6(a–e) shows the propan-2-ol response characteristics of the Zn-doped SnO_2 nanoparticles. As compared to the undoped sample, the response is found to be less in the 1 at% and 2 at% Zn-doped samples, and more in case of the 3 at% and 4 at% Zn-doped samples at all the operating temperatures for all the concentrations. Maximum response 94.5% is observed in this case at 250 °C for 50 ppm concentration. It is observed that at a particular operating temperature, the response increases with concentration, implying sufficient availability of adsorbed oxygen species on the sample surface. In this case the possible reaction mechanism may be written as follows [30]:

$$(CH_3)_2CHOH(gas) + O^- \rightarrow (CH_3)_2CO + H_2O + e^- \quad (15)$$

$$(CH_3)_2CO + O(bulk) \rightarrow CH_3CH_2COOH + O(vacancies) \quad (16)$$

In this case propionaldehyde is first formed due to oxidation which later oxidized to propanoic acid, creating oxygen vacancies in the system and therefore the sample resistance decreases.

3.2.4. Comparison of alcohol sensing

For comparison of alcohol sensing, we have examined the responses of the 4 at% Zn-doped sample as it exhibits the maximum response to methanol, ethanol and propan-2-ol. Fig. 7(a–c) shows the response characteristics of the 4 at% Zn doped sample as a function of alcohol concentration at three different operating temperatures viz. 150 °C, 200 °C and 250 °C. It is clear from the figure that at the lower operating temperatures of 150 °C and 200 °C, the response to propan-2-ol is more than those to methanol and ethanol for all the concentrations. This is attributed to the fact that the alcohols with increased $–CH_2–$ groups are more easily decomposed and oxidized than those with fewer one [31,32]. Therefore, propan-2-ol having the maximum number of $–CH_2–$ groups is easily decomposed and thus reacts effectively with the adsorbed oxygen species, causing release of electrons which, in turn, increases the response.

The transient response characteristics of the 4 at% Zn-doped sample for 50 ppm concentration at three different operating temperatures of 150 °C, 200 °C and 250 °C are shown in Fig. 8(a–c). It is observed that at 150 °C, the response time is least for ethanol, followed by methanol and propan-2-ol respectively while at 200 °C, the response time is minimum for propan-2-ol and it is equal for both methanol and ethanol. At 250 °C, the

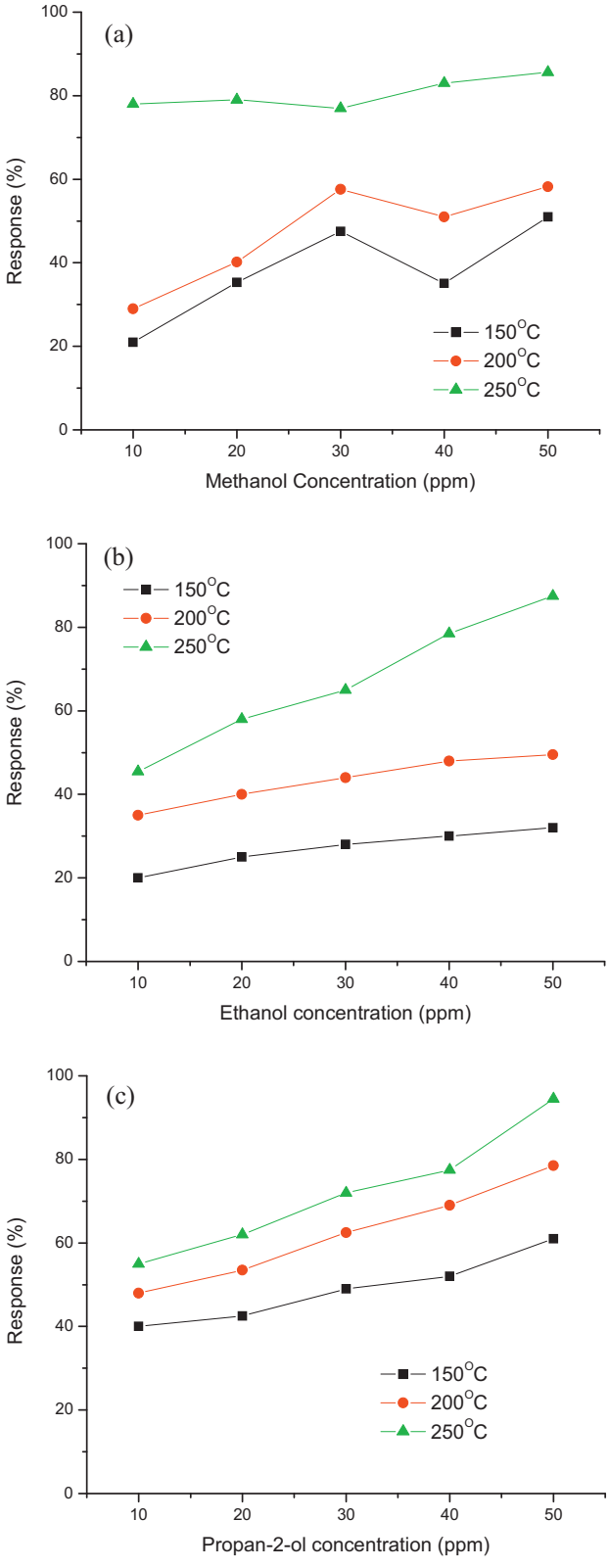

Fig. 7. (a–c) Response characteristics of the 4 at% Zn-doped sample as a function of different alcohol concentration at three operating temperatures 150 °C, 200 °C and 250 °C.

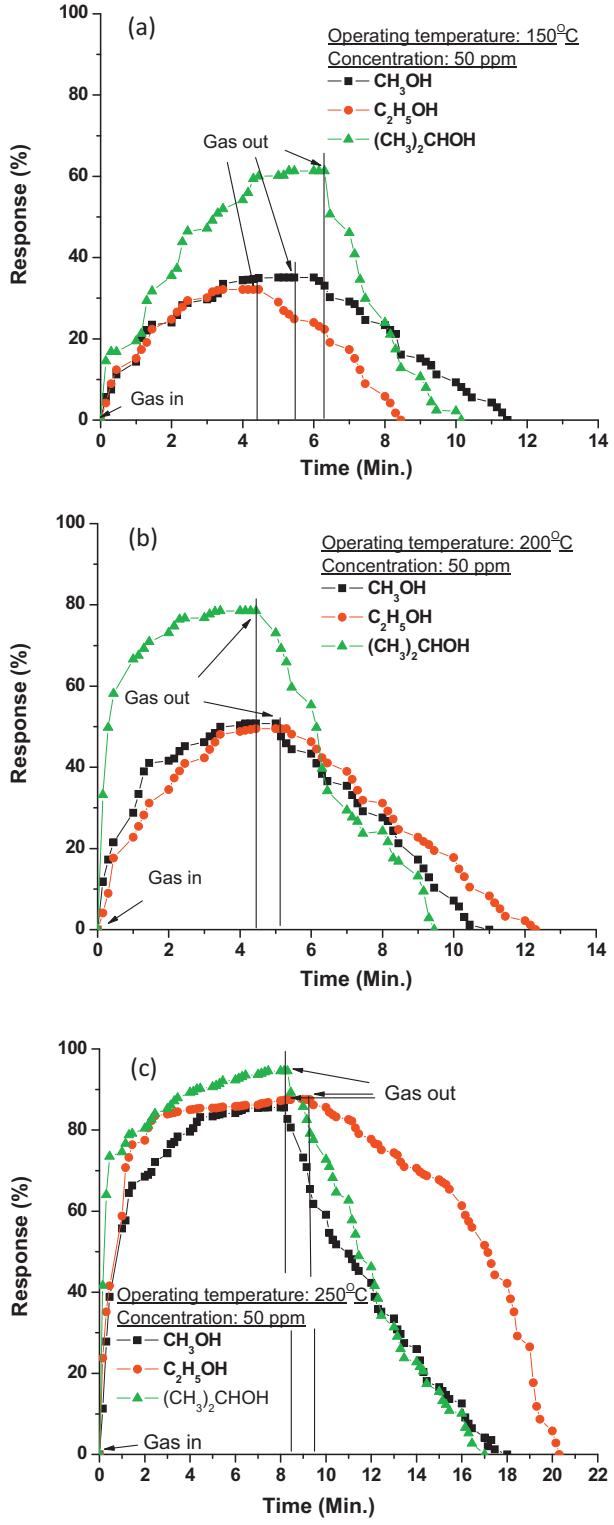

Fig. 8. (a–c) Transient response characteristics of the 4 at% Zn-doped sample for 50 ppm concentration at three different operating temperatures of 150 °C, 200 °C and 250 °C.

response time is found to be minimum and equal for both propan-2-ol and methanol. The response time depends on many factors like the molecular weight of the detected gas or vapour, the operating temperature which influence the chemical reactivity of the detected gas with the adsorbed oxygen species, etc. [33].

4. Conclusion

The Zn-doped SnO_2 nanoparticles synthesized by the chemical co-precipitation route are found to have tetragonal rutile structure with crystallite sizes in the range 10–25 nm. The SAED pattern reveals the different Debye rings of SnO_2, as analyzed in XRD. On investigation of the alcohol sensing properties of the Zn-doped nanoparticles for various concentrations of methanol, ethanol and propan-2-ol at different operating temperatures, it is concluded that the 4 at% Zn-doped sample exhibit the best response to different alcohol vapors at the operating temperature of 250 °C. For a concentration of 50 ppm, the 4 at% Zn-doped sample shows the maximum response 85.6% to methanol, followed 87.5% to ethanol and 94.5% to propan-2-ol respectively at the operating temperature of 250 °C. Higher response to propan-2-ol is attributed to the fact that the alcohols with increased $–CH_2–$ groups are more easily decomposed and oxidized than those with fewer one.

Acknowledgements

Authors are grateful to the Head, Department of Metallurgical Engineering and Material Science, Indian Institute of Technology Bombay, India for providing XRD facilities, and the Director, Sophisticated Instrumentation Centre for Applied Research and Testing, Vallabh Vidya Nagar, Anand, India for TEM characterization. The financial support provided by the Department of Science & Technology, Govt. of India, in the form of a research project (No. SR/S2/CMP-41/2008) is gratefully acknowledged.

References

[1] Y. Zhang, K. Yu, G. Li, D. Peng, Q. Zhang, F. Xu, W. Bai, S. Ouyang, Z. Zhu, Synthesis and field emission of patterned SnO_2 nanoflowers, Mater. Lett. 60 (2006) 3109–3112.
[2] M. Kojima, F. Takahashi, K. Kinoshita, T. Nishibe, M. Ichidate, Transparent furnace made of heat mirror, Thin Solid Films 392 (2001) 349–354.
[3] J.H. Lee, N.G. Park, Y.J. Shin, Nano-grain SnO_2 electrodes for high conversion efficiency SnO_2–DSSC, Solar Energy Mater. Solar Cells 95 (2011) 179–183.
[4] C.G. Granqvist, Transparent conductors as solar energy materials: a panoramic review, Solar Energy Mater. Solar Cells 91 (2007) 1529–1598.
[5] F. Hellegouarc'h, F. Arefi-Khonsari, R. Planade, J. Amouroux, PECVD prepared SnO_2 thin films for ethanol sensors, Sens. Actuators B 73 (2001) 27–34.
[6] Y. Shimizu, T. Maekawa, Y. Nakamura, M. Egashira, Effects of gas diffusivity and reactivity on sensing properties of thick film SnO_2-based sensors, Sens. Actuators B 46 (1998) 163–168.
[7] Y.-S. Choe, New gas sensing mechanism for SnO_2 thin-film gas sensors fabricated by using dual ion beam sputtering, Sens. Actuators B 77 (2001) 200–208.
[8] T.P. Hülser, H. Wiggers, F.E. Kruis, A. Lorke, Nanostructured gas sensors and electrical characterization of deposited SnO_2 nanoparticles in ambient gas atmosphere, Sens. Actuators B 109 (2005) 13–18.
[9] G. Wang, Y. Yang, Q. Mu, Y. Wang, Preparation and optical properties of Eu3+-doped tin oxide nanoparticles, J. Alloys Compd. 498 (2010) 81–87.
[10] H. Liu, S. Gong, Y. Hu, J. Zhao, J. Liu, Z. Zheng, D. Zhou, Tin oxide nanoparticles synthesized by gel combustion and their potential for gas detection, Ceram. Int. 35 (2009) 961–966.

[11] Z. Yu, S. Zhu, Y. Li, Q. Liu, C. Feng, D. Zhang, Synthesis of SnO_2 nanoparticles inside mesoporous carbon via a sonochemical method for highly reversible lithium batteries, Mater. Lett. 65 (2011) 3072–3075.
[12] G. Neri, A. Bonavita, G. Micali, N. Donato, F.A. Deorsola, P. Mossino, I. Amato, B. De Benedetti, Ethanol sensors based on Pt-doped tin oxide nanopowders synthesised by gel-combustion, Sens. Actuators B 117 (2006) 196–204.
[13] P. Ménini, F. Parret, M. Guerrero, K. Soulantica, L. Erades, A. Maisonnat, B. Chaudret, CO response of a nanostructured SnO_2 gas sensor doped with palladium and platinum, Sens. Actuators B 103 (2004) 111–114.
[14] T. Zhang, L. Liu, Q. Qi, S. Li, G. Lu, Development of microstructure In/Pd-doped SnO_2 sensor for low-level CO detection, Sens. Actuators B 139 (2009) 287–291.
[15] B. Thomas, S. Benoy, K.K. Radha, Influence of Cs doping in spray deposited SnO_2 thin films for LPG sensors, Sens. Actuators B 133 (2008) 404–413.
[16] X. Ding, D. Zeng, C. Xie, Controlled growth of SnO_2 nanorods clusters via Zn doping and its influence on gas-sensing properties, Sens. Actuators B 149 (2010) 336–344.
[17] D.-S. Lee, J.-K. Jung, J.-W. Lim, J.-S. Huh, D.-D. Lee, Recognition of volatile organic compounds using SnO_2 sensor array and pattern recognition analysis, Sens. Actuators B 77 (2001) 228–236.
[18] A.C. Bose, P. Balaya, P. Thangadurai, S. Ramasamy, Grain size effect on the universality of AC conductivity in SnO_2, J. Phys. Chem. Solids 64 (2003) 659–663.
[19] O.K. Varghese, L.K. Malhotra, G.L. Sharma, High ethanol sensitivity in sol–gel derived SnO_2 thin films, Sens. Actuators B 55 (1999) 161–165.
[20] R.R. Kasar, N.G. Deshpande, Y.G. Gudage, J.C. Vyas, R. Sharma, Studies and correlation among the structural, optical and electrical parameters of spray-deposited tin oxide (SnO_2) thin films with different substrate temperatures, Physica B 403 (2008) 3724–3729.
[21] H.-C. Chiu, C.-S. Yeh, Hydrothermal synthesis of SnO_2 nanoparticles and their gas-sensing of alcohol, J. Phys. Chem. C 111 (2007) 7256–7259.
[22] B.D. Cullity, Elements of X-ray Diffraction, Addison–Wesley, New York, 1978.
[23] A.S. Riad, S.A. Mahmoud, A.A. Ibrahim, Structural and DC electrical investigations of ZnO thin films prepared by spray pyrolysis technique, Physica B 296 (2001) 319–325.
[24] M. Abdullah Dar, K. Mujasam Batoo, V. Verma, W.A. Siddiqui, R.K. Kotnala, Synthesis and characterization of nano-sized pure and Al-doped lithium ferrite having high value of dielectric constant, J. Alloys Compd. 493 (2010) 553–560.
[25] H. Gonga, J.Q. Hua, J.H. Wang, C.H. Onga, F.R. Zhub, Nano-crystalline Cu-doped ZnO thin film gas sensor for CO, Sens. Actuators B 115 (2006) 247–251.
[26] S. Mishra, C. Ghanshyam, N. Ram, S. Singh, R.P. Bajpai, R.K. Bedi, Alcohol sensing of tin oxide thin film prepared by sol–gel process, Bull. Mater. Sci. 25 (2002) 231–234.
[27] P.P. Sahay, R.K. Nath, Al-doped ZnO thin films as methanol sensors, Sens. Actuators B 134 (2008) 654–659.
[28] P.P. Sahay, S. Tewari, S.J. ha, M. Shamsuddin, Sprayed ZnO thin films for ethanol sensors, J. Mater. Sci. 40 (2005) 4791–4793.
[29] C.S. Prajapati, P.P. Sahay, Alcohol-sensing characteristics of spray deposited ZnO nano-particle thin films, Sens. Actuators B (2011), doi:10.1016/j.snb.2011.09.023.
[30] W.Ya. Suprun, D. Kießling, T. Machold, H. Papp, Oxidation of acetaldehyde and propionaldehyde on a VO_x/TiO_2 catalyst in the presence of water vapor, Chem. Eng. Technol. 29 (2006) 1376–1380.
[31] M.R. Islam, N. Kumazawa, M. Takeuchi, Titaniumdioxide chemical sensor working with AC voltage, Sens. Actuators B 46 (1998) 114–119.
[32] N. Kumazawa, M.R. Islam, M. Takeuchi, Photoresponse of a titanium dioxide chemical sensor, J. Electroanal. Chem. 472 (1999) 137–141.
[33] M. Vrňata, V. Myslík, F. Vysloužil, M. Jelínek, J. Lančok, J. Zemek, The response of tin acetylacetonate and tin dioxide-based gas sensors to hydrogen and alcohol vapours, Sens. Actuators B 71 (2000) 24–30.